Gravity currents descending a ramp in a stratified tank

By J. J. MONAGHAN[1], R. A. F. CAS[1], A. M. KOS[1]
AND M. HALLWORTH[2]

[1]Department of Mathematics, Monash University, Clayton Victoria 3168, Australia

[2]Department of Applied Mathematics and Theoretical Physics, University of Cambridge,
Silver Street, Cambridge CB3 9EW, UK

This paper describes experiments and numerical simulations of a gravity current flowing down a ramp in a tank stratified in two layers. We study the dynamics of the configuration for different densities of the gravity current and different ramp angles. The experiments show that waves of large amplitude can be generated easily and that, depending on the density of the gravity current, the initial gravity current splits into a gravity current along the interface of the stratified layers, and a gravity current along the bottom of the tank. We also describe numerical simulations which give results in agreement with the results of the experiments and enable us to study three-fluid configurations with wider ranges of density than is possible in the laboratory.

1. Introduction

A gravity current is the flow of a fluid of one density into another fluid of different density under the influence of gravity. The discharge of a river into the ocean, sea breeze fronts, and thunderstorm outflows are all examples (Simpson 1987). For gravity currents involving initially homogeneous fluids a wide range of laboratory experiments have been used to investigate the dynamics. The most detailed experiments are for horizontal, essentially two-dimensional, flows with fluid of high density released from a lock in a rectangular tank (Simpson & Britter 1979; Huppert & Simpson 1980; Rottman & Simpson 1983; see Simpson 1987 for further references).

In many geophysical situations the slope of the bottom boundary varies significantly. It is therefore natural to generalize the horizontal gravity current experiments to flow down a ramp in a homogeneous ambient fluid. The most detailed experiments for this configuration are by Britter & Linden (1980) who found, in particular, that the mixing at the head increased dramatically with slope while the velocity of the current remained nearly constant.

Rivers discharging into the Mediterranean with its deep saline pools, and volcanic ash flow through the atmosphere into the ocean are examples of gravity currents in a strongly stratified fluid. With these examples in mind we generalize the experiments of Britter & Linden by replacing the homogeneous fluid in their tank by a stratified fluid with a layer of fresh water overlying a layer of salty water (see Monaghan 1996 for a preliminary report of these experiments). Of particular interest is the behaviour of the gravity current when it encounters the interface where we find substantial waves can be generated and, in some circumstances, the descending gravity current splits into one current along the interface and one along the bottom of the tank.
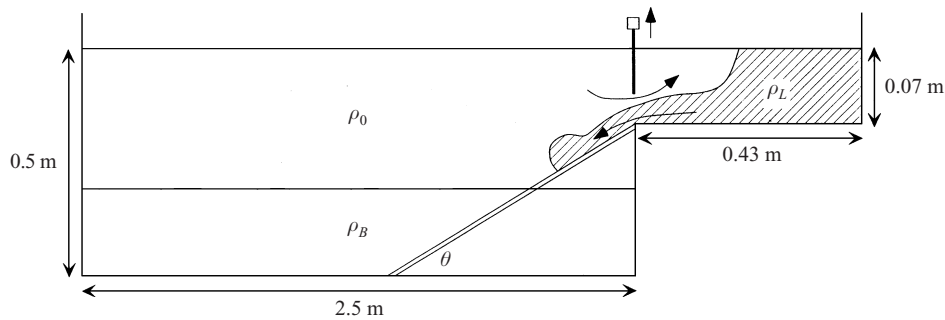
FIGURE 1. A sketch, not to scale, of the experimental setup.

It is difficult, and expensive, to set up experiments with densities much greater than can be produced by dissolved salt, or to change the dimensions and geometry of the tank to correspond more accurately to actual topography. Reliable numerical simulations, bench marked by experiment and other tests, provide a means of studying complicated geophysical conditions. In this paper we use a flexible particle method to study gravity currents flowing down ramps for a wider range of parameters than used in the experiments. The method has been tested and used for problems in gas and high-speed metal impacts but we describe further tests here for problems related to the dynamics of gravity currents.

2. The experimental setup

The experimental setup (figure 1) consists of a tank 2.5 m long, 0.50 m high, and 0.15 m wide. At the end of the main tank a side tank (the lock) is fixed and fluid from it can enter the main tank once a vertically sliding gate is raised. The depth of salty water (density ρ_L) in the lock was 7 cm and its length is 45 cm. The main tank was set up with a bottom layer of salty water (density ρ_B) overlain by a layer of fresh water (density ρ_0). The bottom layer was dyed for easy recognition in slides and videos, and the salty water from the lock was dyed a contrasting colour. The lock is located near the top of the tank, above the interface between the fresh water and salty water in the main tank. The fluid released from the lock reaches the interface by flowing down a ramp (whose angle can be adjusted) which extends from the lock to the bottom of the main tank. In some experiments the ramp was removed so that the end of the tank acted as a vertical ramp. The speed of the descending current, the dimensions of its head, and the amplitude and speed of any waves initiated at the interface were measured from the slides and videos using a fixed background grid of 10 cm squares as a scale. Measurement requires a ruler reading to mm, and a digital clock measuring to 0.01 s.

When the lock gate is removed the salty water from the lock flows down the ramp and fresh water flows into the lock to replace it. Until the fresh water reaches the end of the lock the flow from the lock maintains a nearly constant velocity and depth at the exit point. The amount of lock fluid entering the tank per unit time is therefore constant. When the fresh water reaches the end of the lock the character of the flow in the lock changes because a bore is set up. This does not affect the results of this paper because the gravity current hits the interface well before the bore affects the flow.

The rate of injection of fluid can be estimated from the theory of the breaking

Exp.	$v_h \, (\mathrm{cm\,s^{-1}})$	$v_h/(g'D)^{1/2}$
C5	20.3	0.76
C6	13.5	0.73
C7	10.0	0.76
M3	8.7	0.61
M4	6.9	0.59
M7	9.3	0.79

TABLE 1. The velocity v_h of the head of the initial gravity current. D is the depth of the lock fluid and g' the effective gravity.

dam (see for example Acheson 1990). This theory assumes that the ratio of the lock depth to length is sufficiently small to allow the shallow water theory (Acheson 1990) to apply. In our experiments the lock is six times longer than it is deep so that shallow water theory should be a good approximation. The shallow water theory predicts that the depth of the outflowing fluid is 4/9 of the initial depth D of the lock fluid, and the average exit velocity is $\frac{2}{3}(g'D)^{1/2}$ where g' is the effective gravity, $g\Delta\rho/\rho$, and $\Delta\rho$ is the density difference between the two fluids. The volume flow rate Q is therefore $\frac{8}{27}(g'D)^{1/2}$. Britter & Linden (1980) found, and it also follows from dimensional analysis, that the velocity of the head v_h is proportional to $(g'Q)^{1/3}$. For a lock of depth D, we then find

$$v_h = k(g'D)^{1/2}, \tag{2.1}$$

where the constant of proportionality k has the theoretical value 2/3 at the exit from the lock. Our experimental value of k for the fully developed gravity current is $\sim 0.7 \pm 0.1$ (see table 1) corresponding to

$$v_h/(g'Q)^{1/3} \sim 1.0 \pm 0.1, \tag{2.2}$$

which is at the lower limit of Britter & Linden's (1980) experimental values.

These theoretical estimates are in good agreement with the measurements of the speed and dimensions of the head of the gravity current during the stage when it descends through fresh water. The theoretical estimate of $4D/9$ for the depth of the current leaving the lock was checked during the experiments, and then measured more accurately from a special experiment designed to study the fluid dynamics within the lock. The experiments give the time-averaged depth at exit as $0.43D$ until the return bore from the counter-flowing fresh water reaches the exit of the lock.

While the Reynolds and Richardson numbers vary throughout the experiment both in space and time we can make rough estimates of their values in particular regions. For the tail of the gravity current, the average velocity is typically around $5\,\mathrm{cm\,s^{-1}}$ and the length scale is around $2\,\mathrm{cm}$ so that the Reynolds number is ~ 1000. The video of the experiments shows that waves travel along the tail of the gravity current but the mixing in the tail is weak. For the motion around the head the length scale is larger and the Reynolds number is ~ 4000. We estimate the initial Froude number of the fluid leaving the lock as ~ 0.7 and in the tail of the gravity current it is ~ 0.1. The Richardson number for the tail of the gravity current (defined as in Ellison & Turner 1959) is $\sim 1.0\Delta\rho_L/50$ where $\Delta\rho_L$ is the difference between the lock water and fresh water density in SI units. Typical experimental values of $\Delta\rho_L$ are $10 < \Delta\rho_L < 100$.

3. The experiments

Experiments were run with two geometrically identical tanks in the Geophysical Fluid Dynamics Laboratories, one at Cambridge (denoted by C in the tables), and one at Monash (denoted by M in the tables). The Cambridge experiments used a tank stratified with a lower layer of salt water with density $1050 \, \text{kg m}^{-3}$ and depth 20 cm, and an upper layer of fresh water and depth 32 cm. The Monash experiments had a lower layer of density $\sim 1030 \, \text{kg m}^{-3}$ and depth 23 cm, and an upper layer of depth 30 cm.

In all cases the velocity and dimensions of the head were measured as the gravity current moved through the fresh water layer. In agreement with the experiments of Britter & Linden (1980), the head rapidly reached a steady velocity. Table 1 gives the speed of the head of the current for some of the experiments. These results are in agreement with (2.1) though the coefficient k varies by 15% partly due to the difficulty of defining the front of the head. The height and length of the head were found to be linearly dependent on the distance of the head down the ramp with coefficients of proportionality which agree with those of Britter & Linden (1980) within 10%. Because the head of the gravity current is the site of strong fluctuations (the video shows continual strong wavy disturbances moving over the head) most of the error is due to the difficulty of defining the height and length of the head.

3.1. *General effects*

Figure 2 shows the interaction between the gravity current and the interface for the case when the water in the lock has a density of $1097 \, \text{kg m}^{-3}$ and the bottom layer in the tank has a density of $1031 \, \text{kg m}^{-3}$ and depth 23 cm. The ramp is at an angle of $20°$.

In figure 2(*a*) we show the system as the descending current meets the interface. The descending gravity current has a characteristic head formed by fluid rising at the front of the head and descending at the rear where it mixes with fresh water and with the fluid in the tail of the gravity current. The vortex produced by this process is more intense if the ramp angle is increased.

If the tank had been filled with just fresh water, or just salty water with the density of the bottom layer, the descending current would have run to the bottom of the tank since, even with mixing, it would be more dense than the ambient fluid. In the present experiment, part of the fluid in the upper part of the head is less dense than the bottom layer and the lower part remains denser. The momentum of the descending current causes it to push through the interface to the bottom of the tank (figure 2*b*, *c*). This process initiates both further mixing and a wave of amplitude 9 cm which is clearly seen in the third frame.

In figure 2(*c*) the first wave is still being formed while buoyant fluid rises to the interface. In figure 2(*d*) the buoyant fluid initiates a second smaller wave and begins to spread across the interface while the denser part of the gravity current moves along the bottom of the tank. Figure 2(*d*) shows an apparent increase in the amplitude of the first wave which is due to the wave being reflected at the end of the tank. This produces a substantial pressure head so that the bottom current stops and retreats until the reflected wave returns and runs up the ramp. There is substantial activity in the tank with the interface wave travelling back and forth. At the end of the experiment there are two layers resulting from the gravity current, one at the interface and one along the bottom.

Similar results were found for all gravity currents with initial density more than a few percent above that of the bottom layer. For example figure 3 shows the same
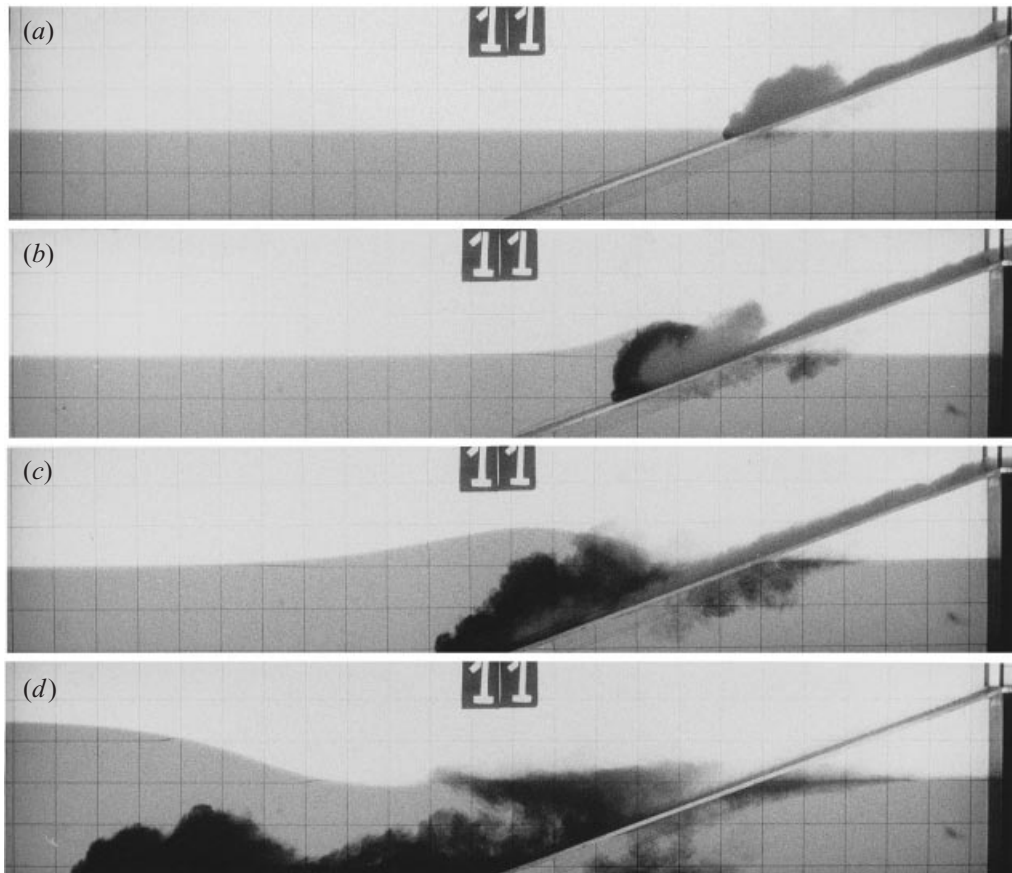
FIGURE 2. Descent of a gravity current of initial density $1097 \, \mathrm{kg \, m^{-3}}$ through a tank stratified with fresh water above and salty water of density $1031 \, \mathrm{kg \, m^{-3}}$ below. The ramp is at $20°$. (*a*) The typical form of the gravity current with its large head and thin tail; (*b*) the first stage of wave initiation; (*c*) the wave is nearly completely formed and the gravity current is descending to the bottom of the tank; (*d*) the wave has moved to the left, and the buoyant material in the gravity current is moving back towards the interface.

tank and the same densities of layers and lock fluid with the ramp at an angle of $90°$. Figure 3(*a*–*c*) shows the descending gravity current striking the interface and initiating the main wave which in this case has an amplitude of 8 cm. Figure 3(*c*) shows that the current hits the bottom of the tank and the video shows that at this stage dense fluid near the right-hand wall is still descending while an adjacent current of buoyant fluid is rising to the surface. The final state is the same as in the previous case.

In figure 4 we show the results of an experiment with the ramp at $20°$ and lock density $1031 \, \mathrm{kg \, m^{-3}}$. The tank density remains as before. In this experiment the momentum of the gravity current carries some of the material into the bottom layer (frames *a* and *b*), but mixing has made all of it buoyant relative to the bottom layer and the mixed lock fluid quickly rises to the interface and runs along it. The gravity current reflects from the end of the tank and returns to run up the ramp. A wave is initiated with amplitude 2.2 cm which is much smaller than for the case with the
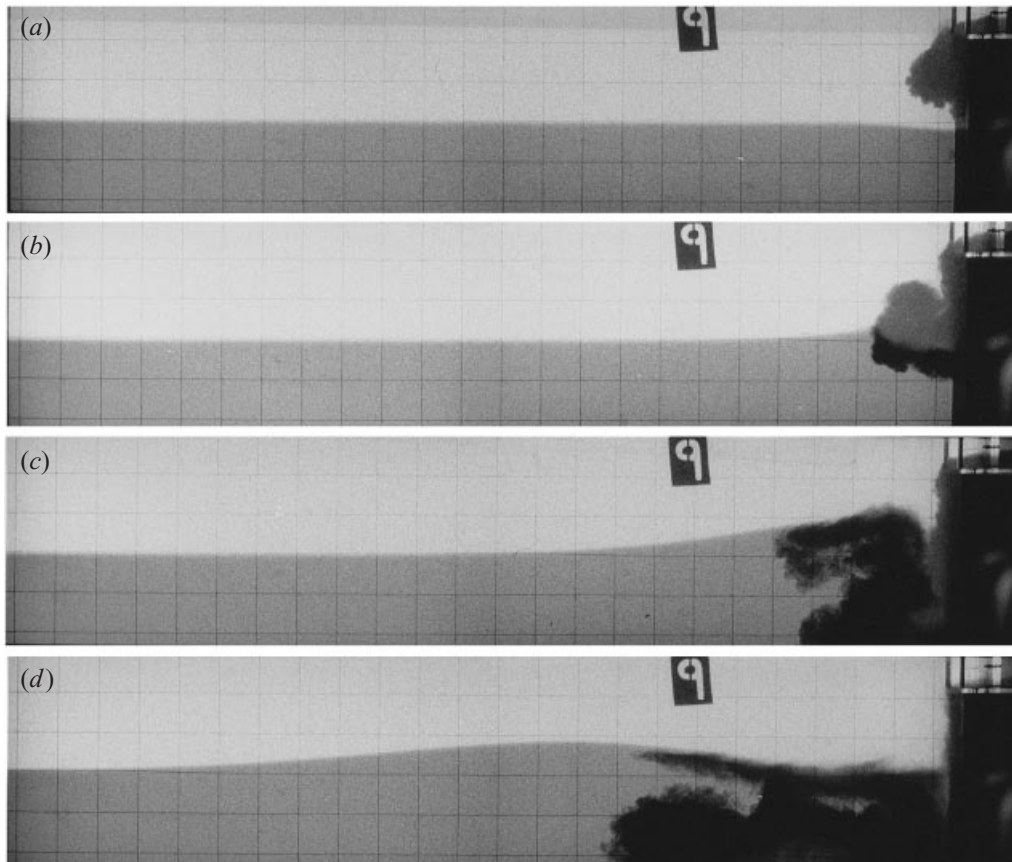
FIGURE 3. The same conditions as for figure 2 except that the ramp has been removed
(equivalent to a ramp at 90°).

denser lock fluid. The final state of the tank consists of the original two layers with
a narrow nearly uniform layer of lock fluid along the interface.

All the experiments, regardless of the angle of the ramp and significant variations
in the density of the bottom layer, show that when the density of the lock fluid is
below that of the bottom layer the gravity current runs along the interface and the
wave amplitude is small. When the density of the lock fluid is a few percent above
that of the bottom layer the gravity current splits into a current along the interface,
and a current along the bottom of the tank. The amplitude of the wave increases as
the density of the lock fluid increases. We discuss this in more detail below.

3.2. *Entrainment*

Entrainment in a horizontal gravity current is complicated and depends on the aspect
ratio of the lock providing the current, the stage (slumping or fully developed) and
the position along the current (Hallworth *et al.* 1996). The theory of Ellison & Turner
(1959) is based on a number of simplifying assumptions and does not attempt to
model the entrainment and growth of the head of the current or its complicated
interaction with a stratified layer. Britter & Linden (1980, p. 541) assume that mixing
processes in the head are essentially the same as in the following flow. Neither the
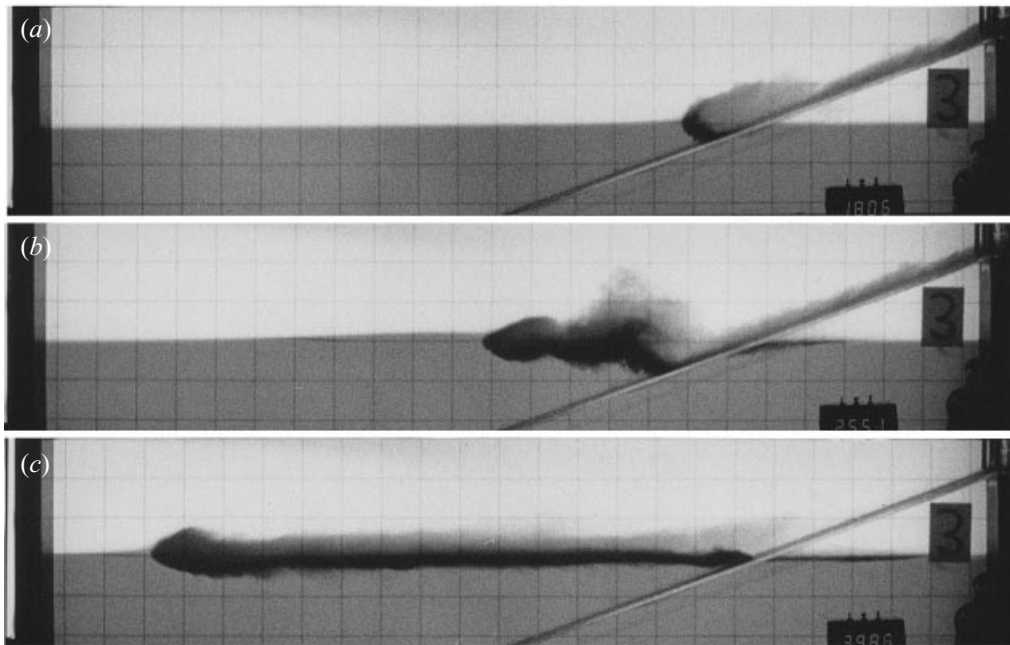
FIGURE 4. Experimental results for the case where the descending fluid has density $1031 \, \text{kg m}^{-3}$, the same as the bottom layer of the tank. The angle of the ramp is 20°. Note the gravity current becomes buoyant with respect to the fluid at the bottom of the tank and runs along the interface. A very small-amplitude wave is generated.

experiments for horizontal currents (Hallworth *et al.* 1996) nor those reported here support that assumption.

Our experiments show that a strong vortex forms at the head of the current as fluid in front of the current flows around the head to enter it alongside the gravity current fluid flowing directly from the lock. If the slope is low (20°), the fluid entering the back of the head largely follows the head so that it appears to be formed around a core of the ambient fluid. This is most easily seen in figure 19 where the low-density fluid, slightly coloured by whisps of brown, is travelling behind the head. If the slope is large (45°), the vortex is more vigorous and the streams entering the head are eventually wrapped up. This process can be seen in figure 21 and in more detail in the numerical simulation shown in figure 22. In addition, as in the case of the horizontal gravity current, the head rises over some of the low-density fluid. By comparison, the following current appears laminar (the Reynolds number is ~ 500).

3.3. *Properties of the waves*

The initiation of the waves by the descending gravity current is analogous to Russell's original demonstration of the generation of a solitary wave (Acheson 1990, p. 64) in which he allowed a solid object to descend into water at one end of a tank. Clear examples of a solitary wave occur in the present series of experiments when the half-width of the wave is less than the distance between the ramp and the end of the tank and only one wave is generated. The formation of a solitary wave is not clear when the density of the lock fluid is too large, as in experiments M9 and M11 (table 2), because the amplitude of the wave is a significant fraction of the depth (typically 40%), and the wave is further distorted by the rising buoyant fluid. At the other

Exp.	Slope (deg.)	$\Delta\rho_L/\rho_0$	$\Delta\rho_B/\rho_0$	a (cm)	$0.4D\Delta\rho_L/\Delta\rho_B$	H (cm)
M4	20	0.027	0.031	2.2	2.4	10
M3	20	0.020	0.031	1.3	1.8	10
M11	20	0.100	0.031	9.0	9.0	10
C9	20	0.100	0.050	6.7	5.6	10
M7	45	0.018	0.027	1.0	1.9	9
M8	45	0.027	0.027	2.0	2.8	11
C5	45	0.100	0.050	5.4	5.6	10
C6	45	0.050	0.050	2.7	2.8	8
C7	45	0.025	0.050	0.7	1.4	11
M9	90	0.097	0.027	8.8	10	17
M10	90	0.027	0.027	2.0	2.8	16
M12	90	0.018	0.027	1.0	1.9	16

TABLE 2. Wave amplitude a and height of head H when the current meets the interface. D is the depth of the lock (7 cm), $\Delta\rho_L$ is the density difference between the lock salty water and fresh water (density ρ_0). $\Delta\rho_B$ is the density difference between the bottom layer and fresh water.

extreme where the wave amplitude is small (~ 1 cm) the structure of the wave cannot be measured accurately. We therefore consider the intermediate case.

As an example consider the experiment C5 with lock density 1100 kg m^{-3} and lower tank layer density 1050 kg m^{-3}. In this case the form of the wave is given approximately by the classical solitary wave relation between amplitude η and distance x (Acheson 1990)

$$\eta = \frac{a}{\cosh^2(x/2b)}, \tag{3.1}$$

where η is the height of the wave above the static level, with the origin of the horizontal coordinate x being measured from the position of the peak of the wave, and

$$b = D_B \left(\frac{D_B + a}{3a}\right)^{1/2}. \tag{3.2}$$

where D_B is the depth of the bottom layer. This theoretical formula, though derived for a wave on a single layer, also applies as a good approximation for a solitary wave on the interface between two layers (Long 1956).

The value of b can be estimated from the width ($x_{1/2}$) of the wave at half-amplitude since, from (3.1), $x_{1/2} = 1.76b$. The experiment gives $x_{1/2} = 40$ cm, so that $b = 23$ cm. This value agrees satisfactorily with the value of 25 cm computed from (3.2) with the experimental values of $a = 5.4$ cm and $D_B = 20$ cm. The experimental speed of this wave is 25 cm s^{-1}. The theoretical value for the speed c of an interfacial solitary wave with layers of depth D_T (top layer) and D_B is given by (Long 1956)

$$c^2 = \frac{g(\Delta\rho)D_T D_B}{\rho(D_T + D_B)}\left(1 + \frac{a(D_T - D_B)}{D_T D_B}\right), \tag{3.3}$$

where $\Delta\rho$ is the density difference between the layers in the tank. For the parameters of the experiment $c = 26$ cm s^{-1}, which is in good agreement with the experimental value of 25 cm s^{-1}.

In table 2 we give the amplitude of the waves for all the experiments and the thickness H of the head of the density current just before it enters the bottom layer.
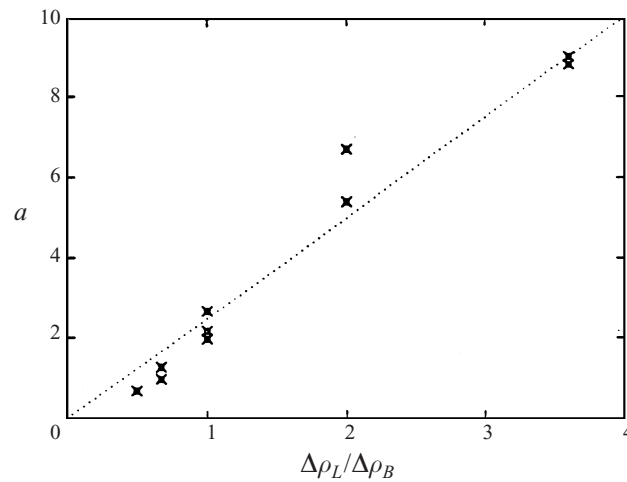
FIGURE 5. The amplitude of the waves a against the ratio of the density difference between the lock fluid and the fresh water $\Delta\rho_L$ and the density difference between the salt water at the bottom of the tank and fresh water $\Delta\rho_B$.

For the largest lock densities two waves are produced and the amplitude refers only to the first wave. Table 2 shows that the amplitude of the wave for fixed tank conditions is not sensitive to the angle of the ramp. For example, the sequences M9 and M11 both produce waves with similar amplitude. The amplitude increases with the density of the lock fluid. These results are summarized in figure 5 where the C and M sequences are combined to show the variation of wave amplitude a with the ratio of $\Delta\rho_L$ and $\Delta\rho_B$ where $\Delta\rho_L$ is the difference between the densities of the lock fluid and fresh water, and $\Delta\rho_B$ is the density difference between the fluid in the bottom layer and fresh water. This figure shows that for fixed tank conditions the amplitude varies approximately linearly with $\Delta\rho_L$.

As a rough approximation for these experiments

$$a \sim 0.4D\frac{\Delta\rho_L}{\Delta\rho_B}, \tag{3.4}$$

where D is the depth of the lock. This quantity is given in the second last column of table 2. The dynamics of the gravity current hitting the interface and initiating a wave is extremely complicated as it involves a downward motion of the head and a flow around the head as fluid in front of the head is forced to move up, around and behind it. We can, however, recover the main features of (3.4) by the following rough argument. The gravity current raises the interface by forcing the fluid in front of it to move up and around the head. The fluid can be expected to move to a height such that the pressure head balances the kinetic pressure. The pressure head is due to the density difference between the bottom and top layers in the tank, and the kinetic pressure is due to the motion produced by the gravity current. This pressure balance condition is

$$g\Delta\rho_B a \sim \rho_0 v_h^2, \tag{3.5}$$

where ρ_0 the average density of the fluid in the head of the gravity current. Our earlier estimate of v_h (2.1) when substituted into (3.5) then gives (3.4). The numerical simulations we describe later use much larger density differences, and a different lock configuration, and they also agree with (3.5).

Table 2 shows that H, the thickness of the head, is approximately constant except for a ramp at angle 90°. This follows from the fact that for our experiments, and those of Britter & Linden, the rate of change of H with distance down the ramp X is given approximately by

$$\frac{\mathrm{d}H}{\mathrm{d}X} = 0.25 \sin \theta. \tag{3.6}$$

Accordingly

$$H = H_0 + 0.25X \sin \theta. \tag{3.7}$$

However, in these experiments all currents drop nearly the same vertical distance before they strike the interface (in the M experiments the drop is 23 cm and in the C experiments it is 25 cm). Taking the drop as the average (24 m), (3.7) predicts that H on striking the interface is

$$H = H_0 + 6. \tag{3.8}$$

We can estimate H_0 as the depth of the current leaving the lock (approximately 3 cm) giving H the value 9 cm which is in satisfactory agreement with the experimental results for the two smaller ramp angles (see table 2). The value of H for the vertical gravity current is different because the current leaving the lock has a large velocity component perpendicular to the ramp and this increases H significantly. In contrast, in the experiments of Britter & Linden, the current was injected parallel to the ramp.

4. Simulations of gravity currents

As in most numerical simulations of geophysical and fluid dynamical phenomena the numerical simulation of gravity currents has involved a variety of approximate models and a variety of integration techniques. The shallow water approximation has been used by Rottman & Simpson (1983), and by Bonnecaze, Huppert & Lister (1993). This approximation has the advantage of simplicity but it cannot model either the detailed motion of the head of the gravity current or the Kelvin–Helmholtz instabilities along the interface.

The early calculations of Daly & Pracht (1968) use the MAC technique to solve the direct Navier–Stokes equations for gravity currents in a horizontal tank. This technique handles discontinuous fluids. Their extensive calculations for free and fixed upper surfaces, a wide range of viscosities, and densities both with and without surface tension are remarkable considering the computing facilities then available. Other examples of MAC calculations for discontinuous fluids are given by Mader (1986).

In addition to the numerical simulations of the laboratory experiments there are numerous calculations of gravity currents in the atmosphere (for problems without initial shear see for example Haase & Smith 1989 and Droegemeier & Wilhelmson 1987, and with shear see Liu & Moncrieff 1996). Their methods are applied to continuous fields appropriate to the atmosphere. They are not accurate for the discontinuous fluids in the laboratory gravity current experiments because they do not preserve the identity of separate fluids as they flow through a cell (the result is significant diffusion across the interface). This is a fundamental problem with the Eulerian finite difference method which can be overcome by front tracking methods or by VOF methods.

The motion of a gravity current is dependent on entrainment of the ambient fluid. As we have seen, the entrainment in the case of ramp flows is complicated, with

different processes occurring in the head and in the following current. In order to simulate the gravity current it is therefore desirable to reduce as much as possible artificial diffusion and artificial mixing terms. In some cases explicit diffusion and dissipative terms are added to model turbulence or to control instabilities. For example the calculations of Hasse & Smith (1989) use diffusion coefficients to model mixing. These diffusion coefficients assume turbulent mixing, but it is clear from the entrainment experiments of Hallworth *et al.* (1996) that constant diffusion coefficients will not model the entrainment in horizontal gravity currents since a major component of the entrainment comes from the current over-riding the ambient fluid, a process which is neither turbulent mixing nor diffusion. This over-riding is also found in ramp flows. Other contributions to the mixing vary significantly along the current so that a diffusion term would require numerical diffusion coefficients which must be obtained from the experiments and varied with space and time. The information required for this detailed modelling is usually not available. Droegemeier & Wilhelmson (1987) introduce both time and spatial smoothing coefficients which are justified by control of numerical instabilities rather than by the correct modelling of mixing and diffusion. Liu & Moncrieff (1996) use the sub-grid turbulence model of Smagorinsky (1963) which has not been shown to correctly reproduce mixing in laboratory gravity current experiments.

In this paper we simulate the experiments using the Lagrangian particle method SPH (Smoothed Particle Hydrodynamics, Gingold & Monaghan 1977, for a review see Monaghan 1992). A brief summary of the method is given in the Appendix. This method has been applied to a wide range of fluid dynamics problems. In the case of gas dynamics involving shock tubes with pressure jumps of 10^5 the method is less efficient than fine-tuned methods based on Riemann solvers but is successful for the Rogers and Sjögreen problems for which many Riemann solver methods fail (Monaghan 1997a). The relativistic version of SPH for gas dynamics (Chow & Monaghan 1997) gives results with the same accuracy as techniques based on finely tuned Riemann solvers (though with slightly less efficiency). SPH is the method of choice for applications to materials which fracture and this can be traced to the fact that the method is Lagrangian (Libersky *et al.* 1993; Benz & Asphaug 1994). Dusty gases, with the dust treated as a second fluid, can also be treated easily with SPH (Monaghan 1997b). SPH has also been applied to free surface flows by replacing the incompressibility condition by a stiff equation of state so that the fluid is slightly compressible (Monaghan 1994). The equation of state is chosen so that the typical Mach number in the flow is 0.1 and, since the density fluctuations depend on the square of the Mach number, the density fluctuations are $\sim 1\%$. This use of an artificial equation of state is equivalent to Chorin's (1967) artificial compressibility method. In all these applications the same method is used with different equations of state and, in the case of relativistic problems, a change to relativistic variables. The simulation of systems with more than one fluid and arbitrary boundaries is straightforward. No other method of which we are aware has been applied successfully, essentially unchanged, to such a wide variety of problems.

The SPH method does not use artificial diffusion or mixing coefficients. Each fluid is represented by designated particles. These particles can exchange momentum through the pressure forces and through the viscosity (which is a Navier–Stokes viscosity). As in all numerical methods there is a limit to the resolution, which in SPH is set by the spacing between the particles. This determines the accuracy and consistency (see the Appendix for more details). Where Kelvin–Helmholtz instabilities occur they can only be modelled accurately down to wavelengths of several particle spacings.

Because the SPH particles can move on scales less than their spacing, they model sub-grid turbulence but the precise details of this are unknown. The result, however, is that particles of one fluid can become mixed with particles of another fluid at interfaces subject to sufficient shear. In this way mixing can occur.

Because all the numerical methods which have been used to simulate gravity currents have errors it is worthwhile discussing the methodology that one can adopt to estimate these errors. Where approximations are made, as in the shallow water approximation used by Rottman & Simpson (1983) and Bonnecaze *et al.* (1993), the justification has been the reasonable agreement of the numerical calculations with experiment. The calculations by Haase & Smith (1989) are not justified by comparing with experiment, but they do examine the sensitivity of their results to some changes of the conditions. Liu & Moncrieff (1996) do not justify their simulations by detailed comparison with experiment though they note qualitative agreement with an idealized problem. Droegemeier & Wilhelmson (1987) do not give detailed comparisons with experiment. They do, however, show that the growth rate of Kelvin–Helmholtz instabilities is in error by approximately 30% and the ratio of amplitude to wavelength differs from experiment by between 14% and 40%. For one set of conditions these authors also consider effects of resolution, but they only show that the higher resolution results give more detail than the coarser resolution. They do not show a converged solution.

The question of errors in CFD computations is complicated. Roache (1997) discusses procedures for establishing errors. Roache (1997) would describe the errors produced when the Navier–Stokes equations are approximated by the shallow water equations as a validation problem, i.e. the correct physics is not being modelled. Thus, when the shallow water equations are applied to a bore then, regardless of how small the time and space steps, the results will be in serious error in the transition from the high to the low water levels in the bore because vertical motion is not described. Similarly the use of diffusion coefficients can incorrectly describe the physics. Verification requires establishing that the equations used are being accurately integrated (they may be the wrong equations but that is a validation issue). Verification is extremely difficult to establish with any certainty. The work of Cheng & Stubin (1978) shows that for the case of Burger's equation the actual error is not predicted from the formal error determined from Taylor expansion of the finite difference terms. Roache (1997) advocates the use of Richardson's technique. This requires combining the results from at least three sequences with different resolution. The key issue is to estimate the order of the errors which may depend not only on the errors from the formal Taylor series but also from the boundary conditions, the use of upwinding, the use of limiters as in TVD and Riemann methods. None of the numerical simulations of gravity currents of which we are aware have verified their methods in the manner advocated by Roache (1997).

Roache's (1997) discussion is primarily aimed at simulations where no extensive laboratory measurements are available as a bench mark. In the present case we do have considerable experimental measurements and these can be used as a bench mark. In addition, by comparison with well-chosen test problems for which very accurate solutions are known, we can establish confidence in our calculations. This is the policy we adopt here.

We describe some of those applications below using the present version of the code. Although the use of a stiff equation of state results in shorter time steps than would be the case with a standard finite difference or finite element scheme, it has a number of advantages. It is explicit, and therefore no iteration is necessary, it is very simple,

so that programming is straightforward and it is very close to the actual physics. The method is not as efficient as boundary element methods when those methods can be used, but it has the advantage that it can be used for more complicated problems.

Because the version of SPH we use has a compressible equation of state leading to a typical Mach number of 0.1 the density can vary by up to $\sim 1\%$. Since much smaller Mach numbers would require a very long calculation with an explicit method, and no implicit version of SPH is known, most of our calculations are for fluid motion with relative density differences in the range $0.07 < \Delta\rho/\rho < 0.40$ which overlap, but are generally larger than, those used in the experiments where $0.03 < \Delta\rho/\rho < 0.10$ (the exception is one simulation to compare directly with the experiments). The simulations, discussed in more detail below, predict results (for example the relation between the velocity of the head and the effective gravity and volume flux, and the relation between the amplitude of the wave and the speed and density of the gravity current) which are in agreement with the experiments.

5. Tests of the simulation technique

In the following we describe tests of the program used for the simulations of our laboratory experiments. The tests begin with the distortion of an elliptical patch which establishes the ability of the technique to follow a free surface. The second test involves the simulation of a jet under gravity. This test establishes that the use of a particle boundary does not affect the flow along and off a surface. The third test is the simulation of a bore. The speed and height ratio shows that the conservation of momentum and energy is accurate and the rolling, overturning motion at the bore jump is replicated. The fourth test is the simulation of horizontal gravity currents which shows that the dynamics of a two-fluid system can be described by SPH. Our fifth test is the simulation of a gravity current descending a ramp in a homogeneous fluid where we show that the results are in agreement with the experiments of Britter & Linden (1980). We refer the reader to Morris & Fox (1997) for an SPH simulation of the growth of a boundary layer resulting from the impulsive motion of a plate. The agreement between theory and numerical experiment is excellent.

5.1. *Distortion of an elliptical patch*

In figure 6 we show an elliptical patch resulting from an initially circular patch of radius 1.0 m with the initial velocity field $(-100x, 100y)\,\mathrm{m\,s^{-1}}$. The condition that the patch remains elliptical with time-varying semi-major axes a and b is that

$$v_x = \frac{x\mathrm{d}a}{a\mathrm{d}t}, \quad v_y = \frac{y\mathrm{d}b}{b\mathrm{d}t}, \tag{5.1}$$

where, for example, v_x is the x-component of the velocity. Conservation of matter for incompressible fluid requires constant ab. From the momentum equation and the condition that the pressure is constant on the elliptical surface, we deduce that

$$\frac{\mathrm{d}A}{\mathrm{d}t} = \frac{A^2(a^4 - \Omega^2)}{a^4 - \Omega^2}, \tag{5.2}$$

where

$$\frac{\mathrm{d}a}{\mathrm{d}t} = -aA \tag{5.3}$$

and Ω is the initial value of ab.

These equations can be solved with high accuracy and compared with an SPH
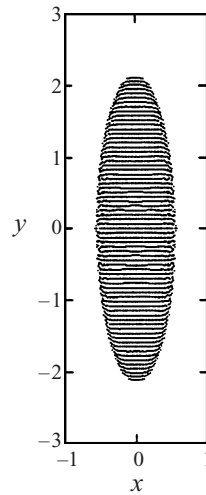
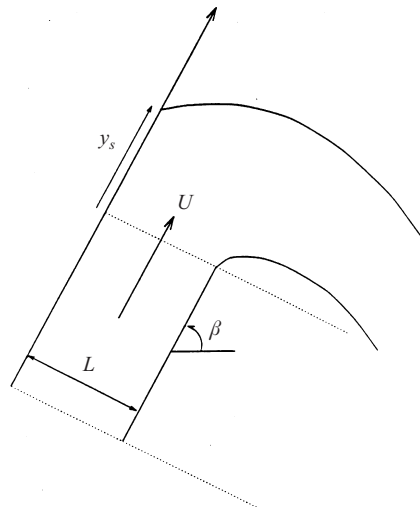FIGURE 6. The SPH particle configuration for an initially circular patch of fluid.

FIGURE 7. The setup for the jet under gravity.

simulation. For this simulation 2000 particles were used and an equation of state with a speed of sound of $1000 \, \text{m s}^{-1}$. Figure 6 shows the SPH particle positions after $0.0093 \, \text{s}$ when the ratio of axes is approximately 4 to 1. The axes agree with the integrations of (5.1) and (5.2) with errors $<2\%$. The density fluctuations are $<1\%$.

5.2. *Jet under gravity*

In this test an inviscid two-dimensional jet issues from an orifice with an upper boundary longer than the lower boundary as shown in figure 7. By using a complex-variable method Dias & Christodoulides (1991) reduced the fluid dynamics equations to a set of equations which could be integrated very accurately. The most difficult parameter to estimate correctly is the position y_s where the upper surface of the fluid leaves the upper part of the boundary. The SPH results for two elevations of the jet are compared with the results of Dias & Christodoulides in figure 8 which shows
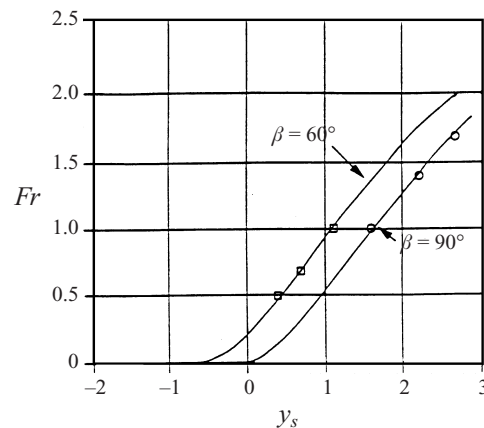
FIGURE 8. A comparison between the SPH results (shown by squares and small circles, and the highly accurate results (Dias & Christodoulides) shown by full lines. The Froude number is denoted by $Fr = U/(gL)^{1/2}$.

the relation between Froude number and y_s. The agreement is very good. The results shown here were first obtained by Monaghan, Thompson & Hourigan (1994). We note that the numerical viscosity is evidently small because of the good agreement between the simulation and the inviscid calculation of Dias & Christodoulides.

5.3. *A bore*

The speed and the jump in height of a bore depends on the conservation of mass and momentum though the shape of the front depends on the dynmnics of the overturning motion. We can expect SPH to get the speed and jump in height correctly because it automatically conserves mass and momentum. It is, however, interesting to see how the dissipation of energy is established through the rolling, breaking motion at the front of the bore.

The bore was set up with stationary fluid with height 20 m in the region $0 < x < 60$ m, and fluid of height 10 m moving to the left with velocity 8.58 m s^{-1}. This initial state is the exact solution of the bore in the shallow water approximation. The equation of state of the fluid was chosen so that the speed of sound is ~ 86 m s^{-1}, and the density fluctuations are $<1\%$.

In figure 9 we show the SPH particles at $t = 5.12$ s when the front has moved forward 45 m. The incoming fluid causes the higher fluid to the left to overturn. Figure 10 shows the bore at 6.83 s when the overturning fluid has bounced off the incoming fluid. This continues with an overturning motion at the front. The speed of the front can only be estimated roughly. From the velocity of the point with maximum height behind the front we estimate the speed as 8.4 m s^{-1} which compares with the value of 8.58 m s^{-1} from shallow water theory.

5.4. *Horizontal gravity currents*

Since the experiments described earlier in this paper require more than one fluid we conducted further tests involving two fluids. We consider a horizontal tank with one section (the lock) containing salty water separated by a partition (the lock gate) from fresh water in the remainder of the tank. In the experiments the lock gate is rapidly pulled from the tank and dense salty water flows under the fresh water. Rottman & Simpson (1983) identified two phases: a rapid adjustment phase followed by the
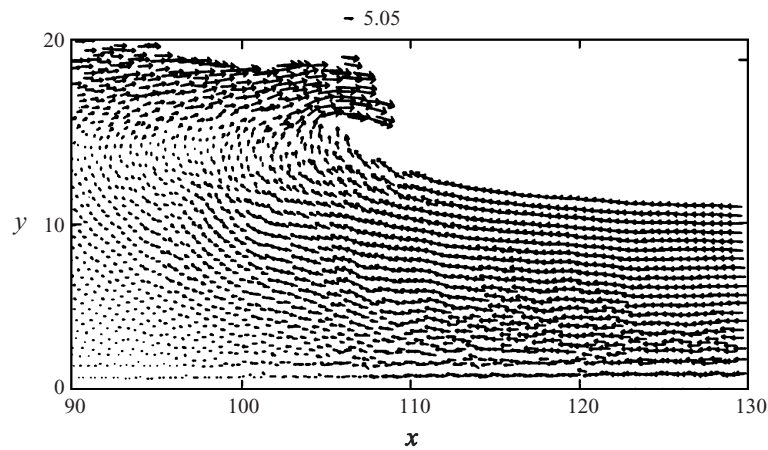
FIGURE 9. The particle positions and velocity field of the bore at time 5.12 s after it has moved forward 45 m from the initial position.
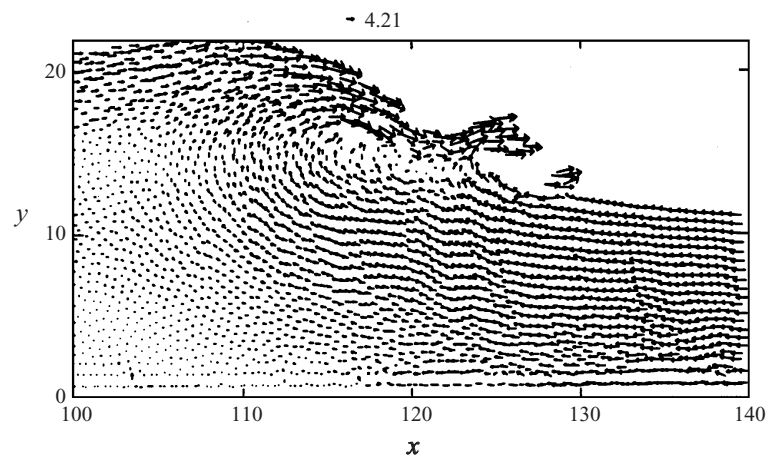

FIGURE 10. The particle positions and velocity field of the bore at time 6.83 s showing the bore front after it has broken and the descending fluid has bounced from the water.

gravity current moving with constant velocity. The counter-current of fresh water into the lock region produces a bore which propagates towards the head of the gravity current. When the bore reaches the head the gravity current slows down.

When the depth of the dense water in the lock is equal to that of the ambient fluid, the experimental measurements of the velocity of the head of the current can be summarized by the formula (Rottman & Simpson 1983)

$$v_h \sim 0.4 \left(gD\Delta\rho/\rho_0 \right)^{1/2}, \tag{5.4}$$

where D is the depth of the tank (and the depth of the lock fluid in these simulations). The experiments do not give details of the internal velocity field of the gravity currents but they do reveal a strong vortex formed at the front of the gravity current and nearly horizontal flow elsewhere. In the following numerical experiments we aim to establish that the speed of the head is in satisfactory agreement with experiment and the qualitative features described above are reproduced.
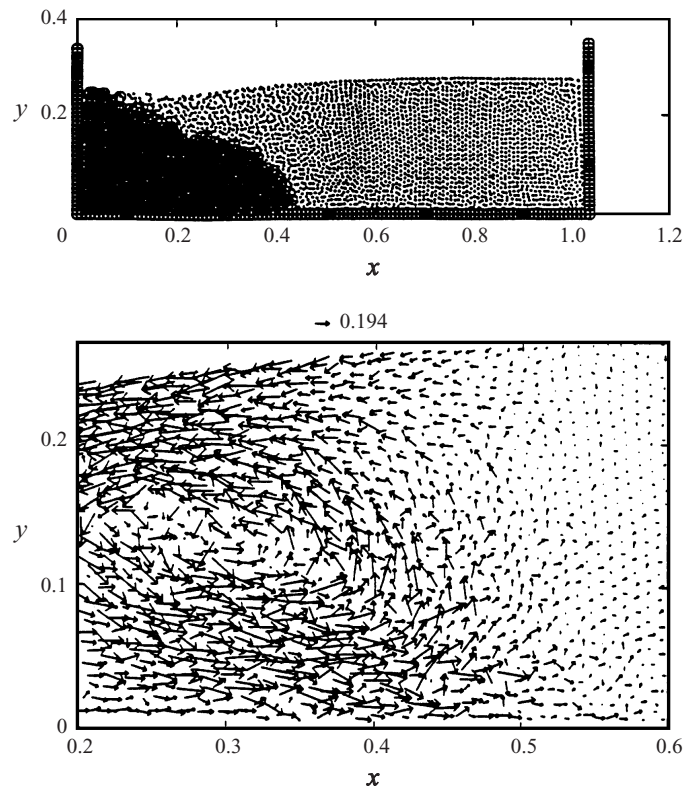
FIGURE 11. The particle configuration and the velocity field for the simulation of a horizontal gravity current at time 1.08 s. The initial lock and tank densities are 1300 and 1000 kg m^{-3} respectively. The initial depth of the fluid is 25 cm and the lock is 25 cm long.

As a typical example of our simulations we show the results for a tank with a fluid of density 1300 kg m^{-3} and a fluid of density 1000 kg m^{-3}. The depth of the fluid in the tank is initially 25 cm, the lock is 25 cm long and the total length of the tank is 100 cm. In figure 11 we show the particle configuration and the velocity field at the head of the current after 1.08 s. The strong vortex roll at the head of the current is clear.

In figure 12 we show the particle configuration and velocity field after 2.15 s. The upper frame shows weak entrainment along the upper surface behind the head and the return bore. The velocity field (shown in the lower frame) indicates that there is negligible entrainment in the head during the early, slumping, phase before the return bore reaches the head, as found experimentally by Hallworth *et al.* (1996).

We have simulated several such tank configurations and in all cases the relation between velocity and density difference is identical to (5.4) except that the coefficient differs by $\sim 10\%$. For the configuration shown in figure 12 the simulation predicts the velocity of the head to be 30 cm s^{-1} which is within the error of the Rottman–Simpson formula which gives 34 cm s^{-1}. In figure 13 we show the particle configuration when the density of the lock fluid is 1200 kg m^{-3}, the lock is 50 cm long and the tank 175 cm long. The behaviour is very similar to that considered earlier.

Examination of the left wall of the tank shown in figures 12 and 13 shows that lock fluid is pinned to the rear wall as the fresh water moves in, and some has been mixed
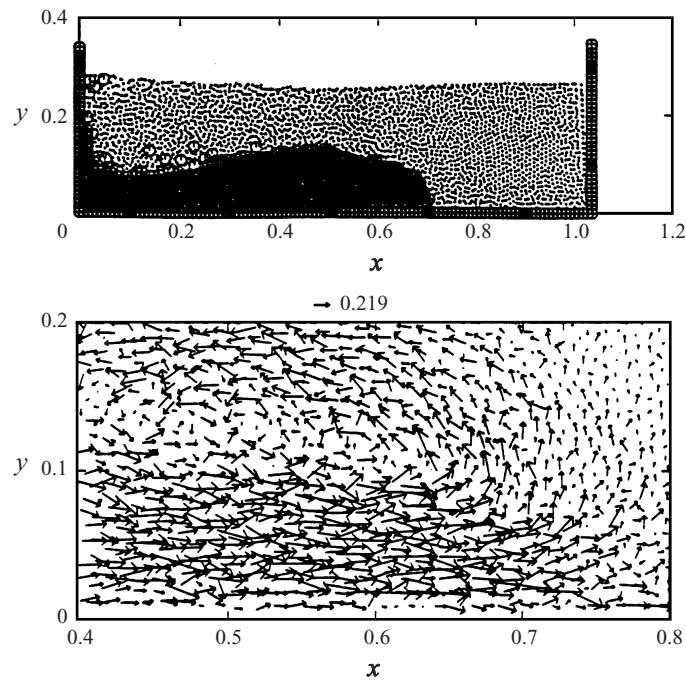
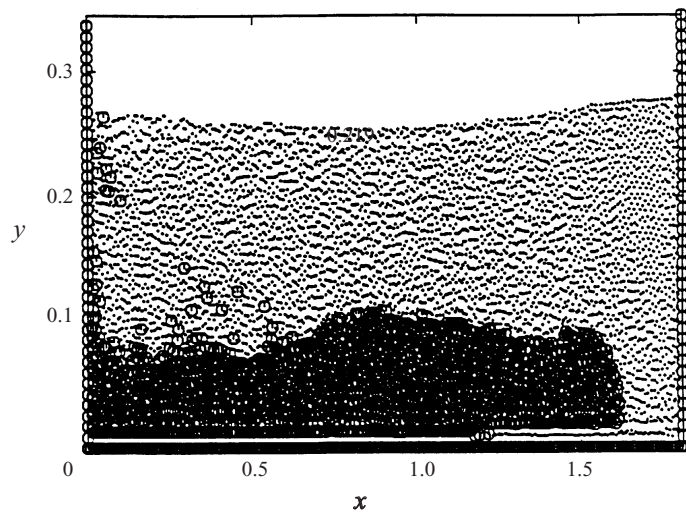FIGURE 12. As for figure 11 but at a later time 2.155 s. Note the return bore.

FIGURE 13. The particle configuration for the simulation of a horizontal gravity current with initial densities 1200 and 1000 kg m^{-3}. The initial depth of the fluid is 25 cm and the lock is 50 cm long. Note that the scale has been expanded.

in the top layer near the left wall. Being surprised by this, because the dense fluid should be below the less-dense fluid, and suspecting the pinned and mixed layers to be a numerical artifact, we ran a special experiment to study the emptying of a lock. This experiment confirmed the numerical simulation. The numerical simulation also shows that the head of the gravity current rides over some of the low-density fluid.

This can also be seen by careful inspection of the photographs of the experiments (see also Simpson 1987).

5.5. *Ramp flow into a homogeneous fluid*

The extensive experiments of Britter & Linden (1980) provide a good bench mark for the numerical calculations. Recent simulations by Cheong & Han (1997) using a Boussinesq approximation are in satisfactory agreement with these experiments.

In the experiments dense fluid flows down a ramp immersed in a tank of fresh water. The dynamics differs considerably from the case of horizontal gravity currents because of the mixing that occurs in the head of the gravity current. The principal results of their experiment is that the velocity of the head is constant to a good approximation, and the velocity is given by (2.2).

In order to confirm that our SPH simulations would reproduce the main features of the experiments we first ran one simulation identical to the experiment with ramp slope 20°. The volume flux Q (actually an area flux for these two-dimensional calculations) is measured by counting the number of lock fluid particles in the lock at each time step. With $\Delta\rho_L/\rho_0 = 0.1$, the simulation gives a gravity current with nearly constant velocity $v_h = 0.72(g'Q)^{1/3}$ which is in good agreement with the experimental relation. The value of Q is $0.0047\,\mathrm{m^2\,s^{-1}}$ which is in reasonable agreement with the theoretical value of 0.0054 using the approximate formula discussed before (2.1). The rate of growth of the head $\mathrm{d}H/\mathrm{d}x$ is $0.2\sin(\theta)$ (where the factor 0.2 has errors of 10% both in the simulation and the experiments because of the disturbances that travel across the head) which is in satisfactory agreement with experiment. These results indicate that SPH is correctly simulating the transfer of momentum between the gravity current and the fluid (otherwise v_h would not become constant, its value would not agree with the experimental relations), and it correctly simulates the way in which the head grows.

Further simulations were run using a lock which is 25 cm deep and 50 cm wide, which is therefore similar to the horizontal lock configuration associated with figure 13. These simulations have larger density differences and larger lock dimensions which imply higher flow velocities. As mentioned earlier this allows our explicit technique to work more efficiently and we can sample from a wider parameter range. The first of these simulation has lock fluid of density $1300\,\mathrm{kg\,m^{-3}}$, and the fluid in the remainder of the tank has density $1000\,\mathrm{kg\,m^{-3}}$. The slope of the ramp is 20°. In figure 14 we show the particle configuration at times 3.16 s and 4.51 s. At the earlier time the characteristic head of the gravity current is clear as is the pinned layer at the end of the lock which we referred to earlier. In this figure the SPH particles for the fluid at the bottom of the tank have been given a different symbol to indicate the motion of the fluid. Figure 15 shows that the velocity field around the head forms a weak vortex with a return flow of ambient fluid into the head.

The second simulation we show is for a ramp at 45°, lock fluid of density $1400\,\mathrm{kg\,m^{-3}}$, and fluid in the remainder of the tank with density $1000\,\mathrm{kg\,m^{-3}}$. In figure 16 we show the particle configuration after 1.05 s. A difference from the flow for the lower ramp angle is that the head has a different shape. In figure 16 we show the configuration at 1.83 s, and this shows very clearly how the fluid in the head becomes distorted by the flow. The dark fluid rising up has the same density as the rest of the fluid in the tank. Its motion reflects the flow around the head of the descending gravity current. The lock shows the features noted before for the horizontal tank, in particular a thin layer of pinned dense fluid and a return bore, and these are also seen in the laboratory experiments.
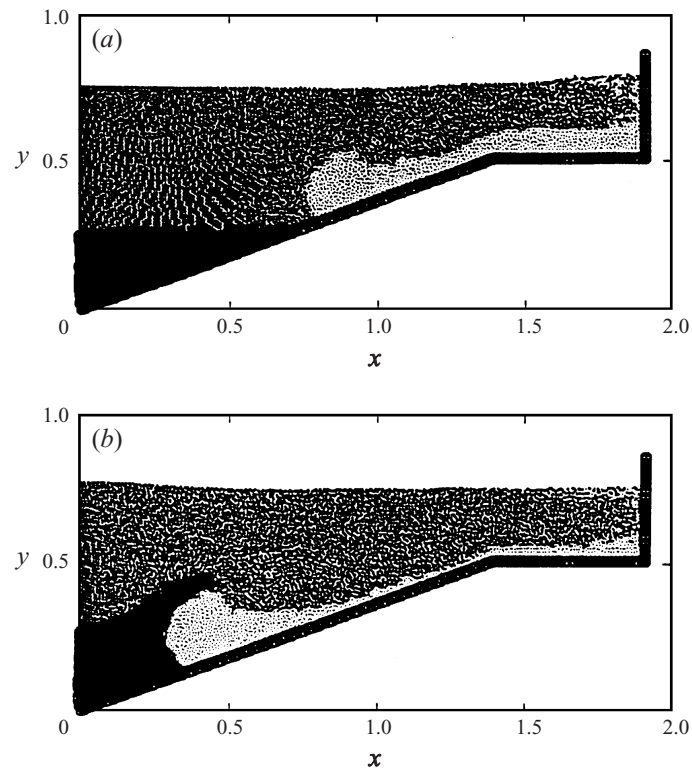
FIGURE 14. The particle configuration for ramp flow into a homogeneous fluid at (*a*) 3.16 s and (*b*) 4.51 s. The lock fluid and the tank densities are 1300 and 1000 kg m^{-3} respectively. Note the characteristic head and the pinned layer at the end of the lock.
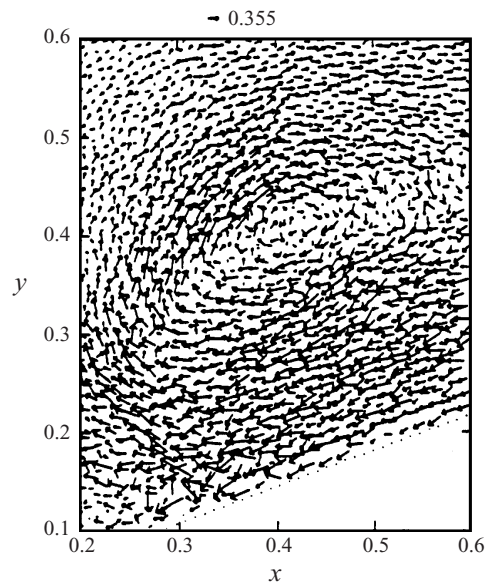

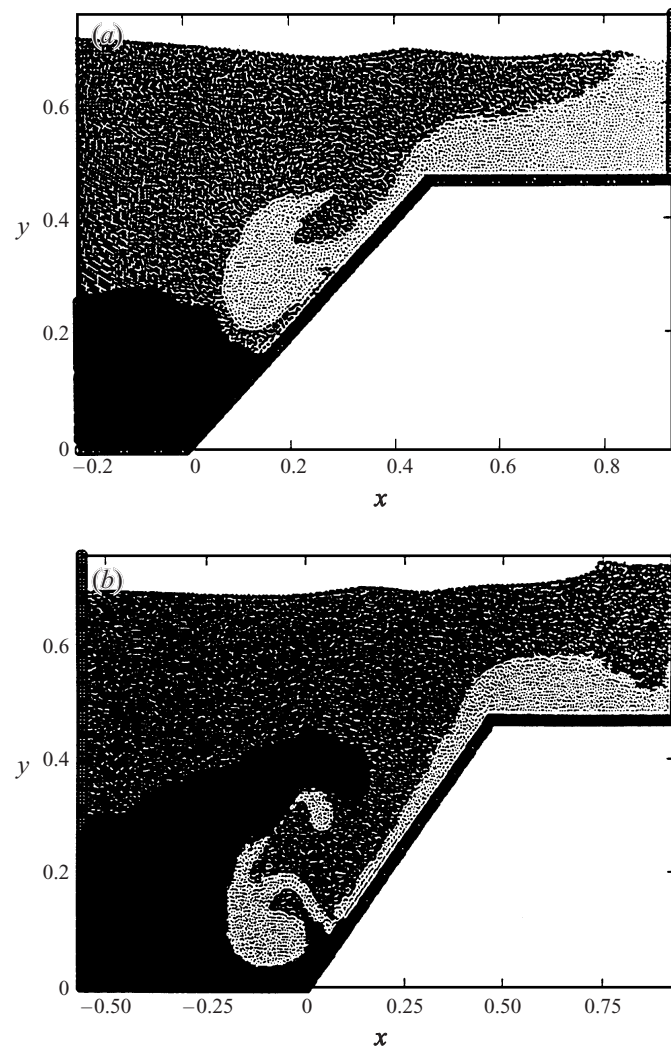FIGURE 15. The velocity field around the head for the gravity current of figure 14.

FIGURE 16. Flow into a homogeneous tank down a ramp at $45°$ with lock and tank densities of 1400 and $1000 \, \text{kg m}^{-3}$. (*a*) The time is 1.05 s. Note the head shape is different from that for the ramp at $20°$. (*b*) the time is 1.83 s. The fluid in the bottom half of the tank is given a different symbol to illustrate how it flows around the head of the gravity current. The vertical and horizontal scales are different.

In table 3 we show the velocity of the head v_h, $\Delta\rho_L$, and the volume flux Q for several simulations. The results are in good agreement with the formula

$$v_h/(g'Q)^{1/3} \sim 0.7, \tag{5.5}$$

which is in satisfactory agreement with our experimental results (summarized by (2.2)) and with the experiments of Britter & Linden (1980) though their coefficient is larger than that from our experiments and simulations.

The value of H for the simulation of figure 14 is 19 cm which is in good agreement with (3.8) since the depth of the flow at exit is $\sim 12 \, \text{cm}$. The value of H for the simulation of figure 15 when the head has dropped 24 cm is 18 cm which is in excellent agreement with (3.8).

θ (deg.)	$\Delta\rho_L$	Q	$v_h/(g'Q)^{1/3}$
20	0.45	0.024	0.75
20	0.40	0.023	0.73
20	0.30	0.023	0.68
20	0.10	0.0047	0.72
45	0.40	0.020	0.72
45	0.30	0.021	0.65

TABLE 3. Speed v_h of the head of the gravity current estimated by SPH simulations for ramp flow into a homogeneous fluid. Q is the flux and $\Delta\rho_L$ is the density difference between the lock and fresh water. The fourth row entry for $\theta = 20°$ is for a lock identical to those in the experiment.
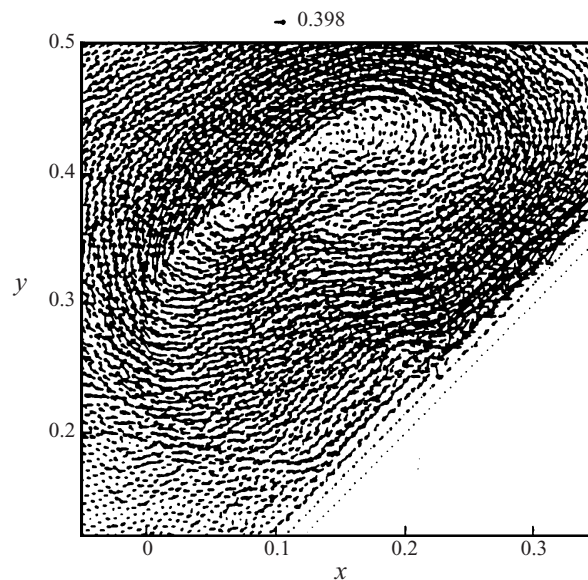

FIGURE 17. The velocity field around the head of the gravity current down a ramp at 45° into a homogeneous fluid. Further details are given in the text.

In figure 17 we show the velocity field around the head of the gravity current. There is a strong vortex motion which carries fresh fluid from around from the front to the rear of the head. This strong motion is clearly seen in videos of the flow. Close examination of those videos shows that the region behind the head is mixed very slightly with the original lock fluid in agreement with our numerical simulations which predict that this fluid is substantially the ambient fluid. This point is also discussed in the next section where the structure of the head is examined when it strikes the interface. If the ramp slope is made greater this vortex motion becomes more vigorous and is the cause of the head becoming distorted and wrapped up.

These result are in general agreement with those of Cheong & Han (1997) though their use of diffusion coefficients is a poor approximation to the entrainment process that actually occurs.

Since the SPH simulation results in the gravity current moving at nearly constant speed with the dependence on Q and g' given by (5.5) we can infer, from the argument used by Britter & Linden (1980), that (the simulation of) the mixing by the influx of

θ (deg.)	$\Delta\rho_B/\rho_0$	$\Delta\rho_L/\rho_0$	a (cm)	a/a^*
20	0.10	0.40	15	1.5
20	0.10	0.30	15	1.8
20	0.07	0.21	13	1.9
20	0.20	0.40	9.6	1.4
45	0.1	0.40	15	1.5
45	0.1	0.30	15	1.8
45	0.3	0.40	11	1.5

TABLE 4. Amplitude a of the waves generated in the SPH simulations for various lock density difference $\Delta\rho_L$, bottom layer density difference $\Delta\rho_B$, and ramp slope θ. The length a^* is defined in the text.

fresh water into the head via the vortex is the primary mixing process determining the speed of the gravity current.

6. Ramp flow in a stratified tank

We now consider the numerical simulation of configurations similar to those of our experiments. The early stage of the experiments, where the descending lock fluid passes through the upper layer of the tank, is equivalent to descent through a homogeneous fluid. In the following we concentrate on the new phenomena arising from the current striking the interface. It will emerge, even more clearly than in the experiments (since the simulation gives us more easily accessible data), that the detailed behaviour depends on the angle of the ramp. For example a ramp at 45° produces a stronger vortex motion at the head of the gravity current than a ramp at 20° and, as a result, there is stronger wrapping of the head when the ramp is steeper. Despite this, the amplitude of the waves is nearly independent of the angle of the ramp, with the other parameters held constant, as shown in table 4, in agreement with experiments. In table 4 the amplitude of the wave is given in term of a^* where

$$a^* = \frac{v_h^2 \rho_0}{\Delta\rho_B g}. \tag{5.5}$$

6.1. *Ramp at 20°*

We first consider flow down a ramp at 20° with lock density $1210\,\mathrm{kg\,m^{-3}}$ and tank densities 1000 (upper layer) and 1070 (lower layer) $\mathrm{kg\,m^{-3}}$. The lock has length 50 cm and depth 25 cm as in the simulations for a homogeneous tank. To reduce computation time we set the left end of the tank at 0.75 m from the bottom of the ramp. We compare this case with experimental results which have the same value of $\Delta\rho_L/\Delta\rho_B$, namely with densities 1097 and $1031\,\mathrm{kg\,m^{-3}}$. We do not expect exact agreement because of the different depth in the lock but we expect qualitative agreement.

In figure 19 we show the experiment and in figure 18 the simulation as the head of the gravity current hits the interface and passes through it. The white region in figure 19 is the fresh water, the red/brown the gravity current and the blue is the bottom salty layer. The dark region near the head is a mixture of blue and red/brown, but it is not clear how much of this is produced by the head being seen through blue fluid remaining on the wall of the tank. Figure 19(*a*) shows that as the head passes through
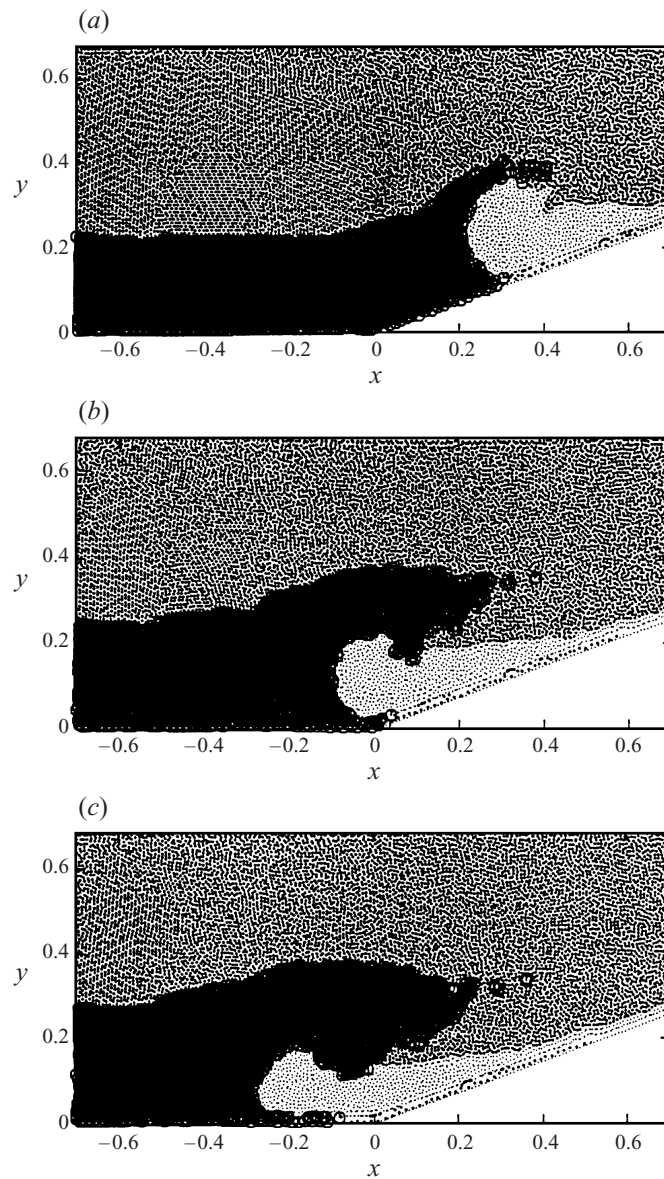
FIGURE 18. The SPH simulation of flow down a ramp at 20° with lock density and bottom layer densities 1210 and 1070 kg m^{-3} respectively. The ratio of density differences is nearly identical to that for the experiment shown in figure 18.

the interface it remains compact with a plug of nearly fresh water following it. Figure 19(b) shows the blue fluid being pushed to what is nearly the peak amplitude. Finally, in figure 19(c) the blue fluid has almost reached the tail of the gravity current. The wave is now almost completely formed.

In both the experiment and the simulation v_h is given by (5.3), and the growth of the head is close to (3.6) giving the satisfactory agreement with experiment noted after (3.8). As in the case of the experiments this simulation combined with other simulations described below shows that the amplitude is not sensitively dependent on the slope of the ramp.
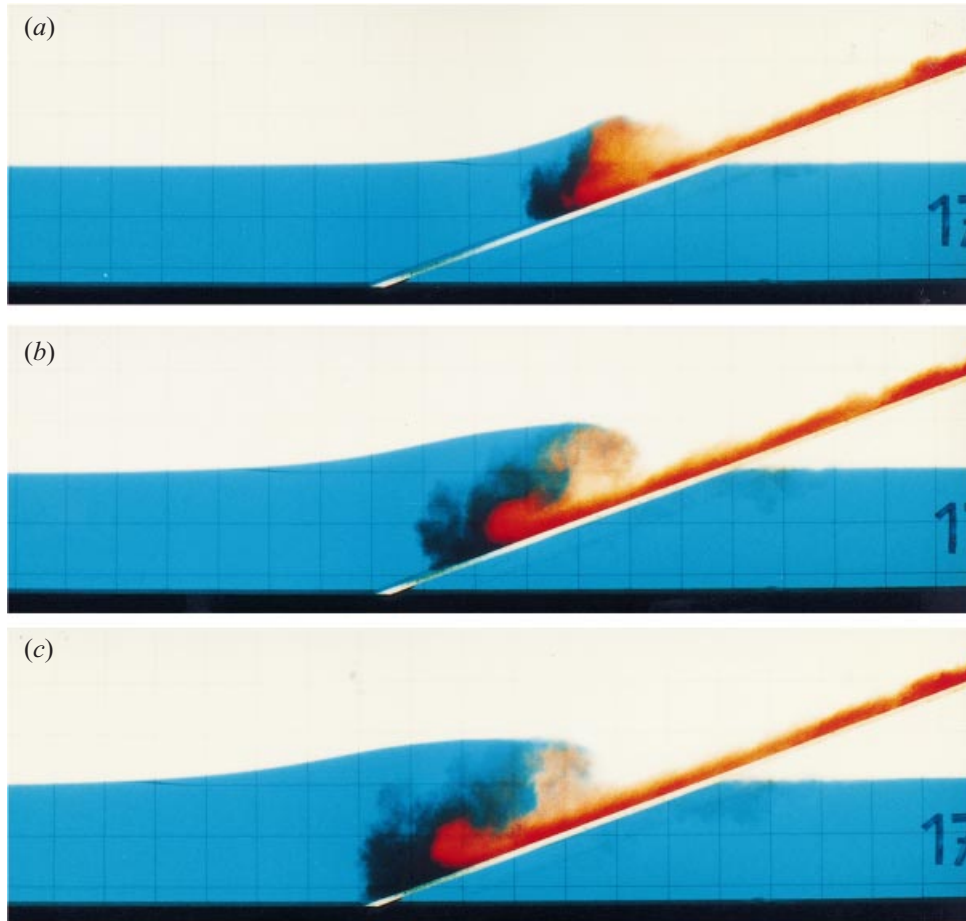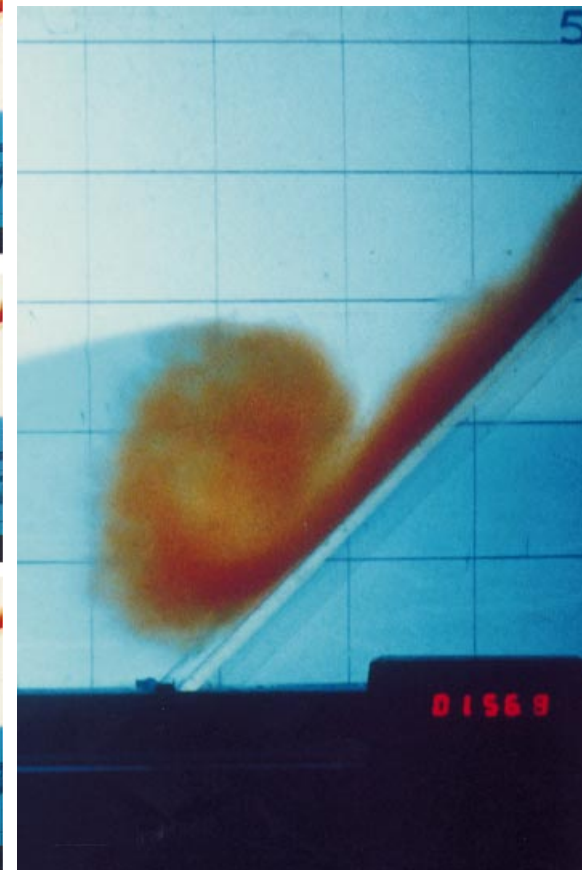
FIGURE 19. For caption see page 64.

FIGURE 21. For caption see page 64.

Gravity currents descending a ramp in a stratified tank
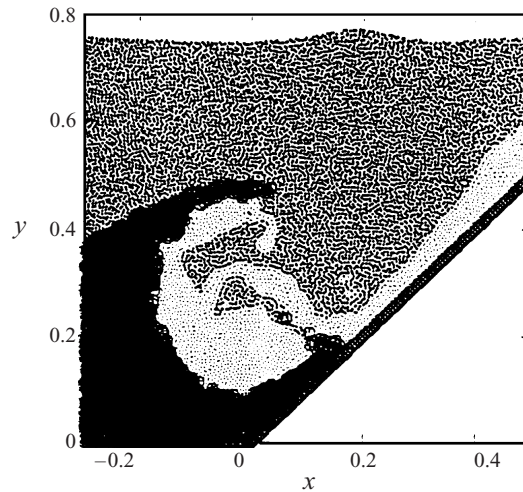
63

FIGURE 20. The SPH simulation for the same configuration shown in figure 20 except that the densities of the lock and bottom layer were 1400 and 1200 kg m^{-3} respectively giving the same ratio of density differences as in figure 21.

6.2. *Ramp at* 45°

We now consider a steeper ramp with lock density 1400 kg m^{-3} and lower tank layer density of 1200 kg m^{-3}. The lock is 25 cm deep and 50 cm long as before. The left boundary of the tank is 0.75 m to the left of the bottom of the ramp. Figure 20 shows the simulation and figure 21 the experiment when the head has penetrated the interface. The head is the site of a strong vortex with fresh water moving around and behind the head, picking up small quantities of the lock fluid and giving the back section of the head a wispy appearance.

On striking the interface the front of the head slows down and begins to spread around the impact zone. The fresh, or nearly fresh, water following becomes wrapped up and this is the origin of the light coloured region in the centre of the head.

The simulation shows many of the features of the experiment: the spreading of the head around the impact zone and the penetration of fresh water into the head. Strong wrapping occurs though we find that the details of the wrapping are sensitively dependent on the resolution. If this is a reasonable picture of what is happening in the experiments then, since they are three-dimensional, we can never expect the two-dimensional simulations to give an accurate picture of the mixing within the head because the thin sheets that are produced can be expected to contort and disrupt across the tank.

6.3. *Lock fluid at low density*

In figure 22 we show the fluid configuration in a simulation where the lock fluid has density 1200 kg m^{-3} and the bottom layer has density 1400 kg m^{-3}. The gravity

FIGURE 19. The current in an experiment with flow down a ramp at 20° into a stratified tank. The lock and bottom layer densities are 1097 and 1031 kg m^{-3} respectively.

FIGURE 21. The head in an experiment with lock and bottom densities of 1100 and 1050 kg m^{-3} respectively, and ramp angle 45°. Note the light coloured central region which is largely fresh water, and not the wrapping of the fluid.

current now runs along the interface with the typical curved front seen in experiments (figure 4). There is substantial entrainment. The speed of this interstitial current varies between 38 and 28 cm s^{-1} which can be compared with the experimental results given by Simpson (1987) from which we estimate the speed as 40 ± 5 cm s^{-1}.

6.4. *Different bottom-layer depths*

One experiment was run with the depth of the bottom layer decreased by 16%. The change in the amplitude was <2%. This result indicates that for this experimental setup the amplitude of the waves is not sensitively dependent on the depth of the bottom layer. To test the effect of deeper bottom layers with all other parameters fixed we ran simulations with $\rho_L = 1400$ and $\rho_B = 1100$. The results are shown in figure 23 where (*a*) is for a bottom layer depth of 33 cm, (*b*) 23 cm, and (*c*) 11 cm. Although the details of the head vary in each case the amplitude of the wave is 15 ± 0.5 cm. This indicates strongly that the depth does not affect the height to which water in the bottom layer is heaved. It is clear, however, that there must be some depth effect since there is no wave if the depth is zero. A detailed study of the influence of depth of the bottom layer on the initiation of waves is beyond the scope of this paper.

7. Discussion and conclusions

7.1. *Laboratory experiments*

The experimental work described in this paper has been concerned with a gravity current travelling down a ramp in a tank with a layer of fresh water above a layer of denser salty water. When the gravity current moves through the first layer the results are in agreement with those of Britter & Linden (1980) for flow through a homogeneous fluid. When the gravity current strikes the interface between the fluid layers in the tank, waves of large amplitude are generated when the initial density of the gravity current is greater than that of the bottom layer. When the density is decreased, the amplitude of the wave generated decreases, and is negligible when the initial density of the gravity current is less than that of the bottom layer. The amplitude of the wave can be estimated by simple dynamical arguments.

The experiments show that most of the entrainment occurs through fluid moving around the head and entering it from behind. The direct stream of gravity current fluid from the lock and the stream of ambient fluid enter the rear of the head alongside each other. If the slope is low (20°) the vortex motion around the head is weaker and the incoming ambient fluid tends to follow the head without substantial wrapping up. If the slope is much steeper (45°) the vortex motion is stronger and substantial wrapping occurs. These effects are predicted by the numerical simulation.

7.2. *Numerical simulations*

The dynamical simulations of horizontal currents and ramp flow into either a homogeneous or a stratified tank, though they involve larger density differences than those in the laboratory experiments, are in good agreement with the relations deduced from experiments, for example with respect to:

(i) the velocity of the head in terms of the effective gravity and the volume flux of the current;

(ii) the variation of the thickness H of the head as a gravity current descends a ramp in a homogeneous fluid;

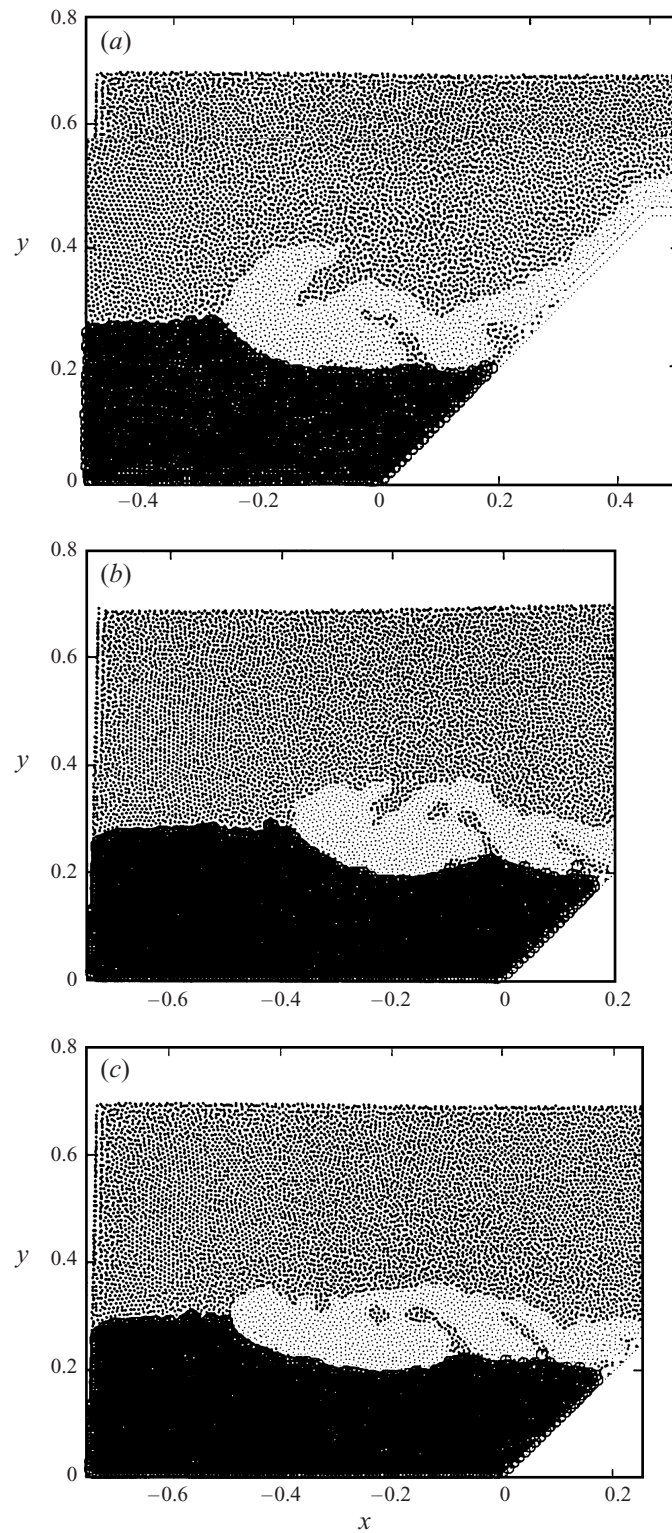(iii) the insensitivity of the speed of the current to the slope of the ramp;

FIGURE 22. The simulation of a gravity current descending a ramp into a stratified tank when the initial density of the gravity current is 1200 and the density of the bottom layer is 1400 kg m^{-3}.
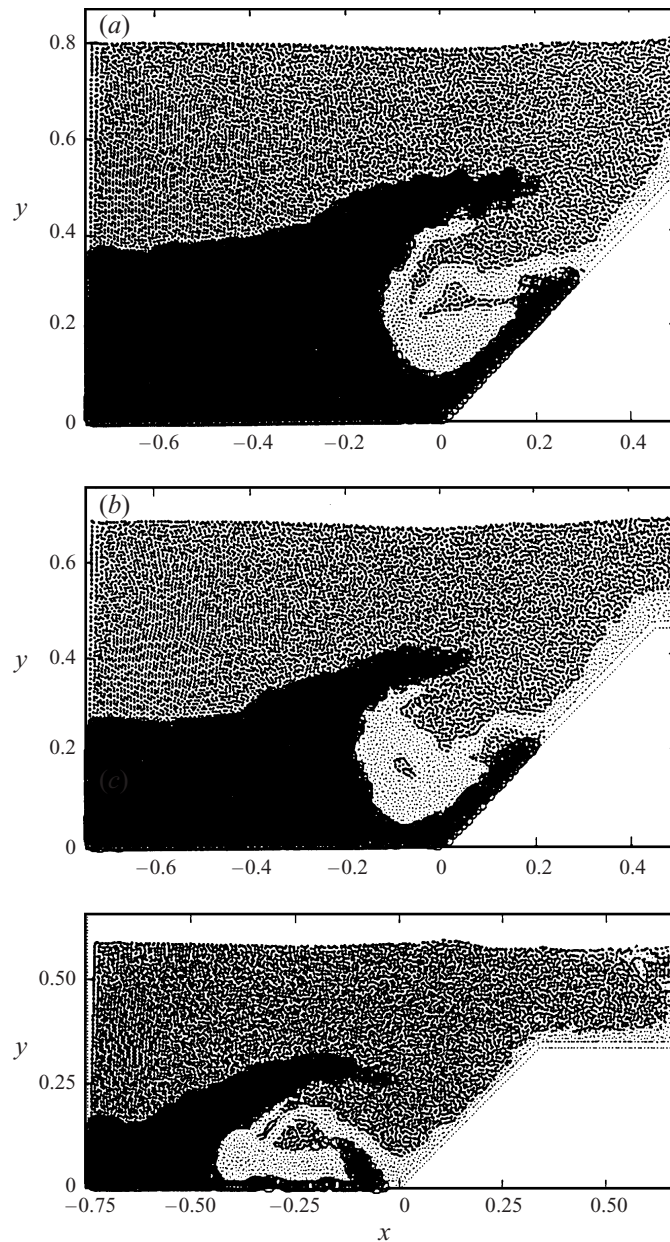
FIGURE 23. SPH simulations of the gravity currents in tanks with different bottom layer depths, (*a*) 33 cm, (*b*) 23 cm, (*c*) 11 cm, all other parameters being kept the same.

(iv) the relation between the amplitude of the wave generated by a gravity descending into a stratified tank and the simple formula (3.5).

The simulations together with videos of the experiment show that the entrainment in the head occurs in two stages. In the first stage currents from the front of the head and directly from the lock enter the head alongside each other and become wrapped up. The wrapped layers eventually break up in the laboratory experiments but in the strictly two-dimensional simulations they do not.

7.3. *Geological significance*

The experiments show that large waves can be initiated easily if there is a large density contrast between the descending gravity current and the bottom layer. For example, according to (3.5), a gravity current moving at $20\,\mathrm{m\,s^{-1}}$ will produce a wave with amplitude $\sim 40\,\mathrm{m}$ if the density difference between the bottom layer and the upper layer is comparable to the density of the gravity current. This situation can be expected to occur frequently for dense pyroclastic flows such as block and ash flows (Cas & Wright 1987, 1991). The experiments and simulations therefore suggest that tsunamis can be generated by the entry of relatively dense pyroclastic flows into the sea, either from vertically collapsing eruption columns, or from relatively low angles of entry ($>20°$) onto the sea surface in agreement with observations of the Krakatau eruption, and speculations concerning the eruption of Santorini in 1600 BC (Monaghan, Bicknell & Humble 1994).

For a pyroclastic flow with a density substantially less than water, the experiments show that the gravity current treats the bottom layer as a nearly rigid surface and runs along it. Very energetic pyroclastic flows are known to have travelled 100 km or more on land so these experiments suggest that the pyroclastic flow reported to have travelled over the sea from Krakatau is not impossible.

Appendix

In this Appendix we briefly describe the SPH technique. The key task is to interpolate from disordered particles. To this end we start with the exact relation for any quantity (scalar, vector or tensor field) B

$$B(\mathbf{r}) = \int B(\mathbf{r}')\delta(\mathbf{r} - \mathbf{r}')\,\mathrm{d}\mathbf{r}', \qquad (A\,1)$$

where the volume element is $\mathrm{d}\mathbf{r}'$. We now approximate (A 1) by replacing the δ-function by a kernel function W which mimics a δ-function. For example it could be a Gaussian. If now we write (A 1) as

$$B(\mathbf{r}) = \int \frac{B(\mathbf{r}')}{\rho(r')} W(\mathbf{r} - \mathbf{r}')\rho(r')\,\mathrm{d}\mathbf{r}' \qquad (A\,2)$$

we can approximate it by imagining the space occupied by the fluid being divided into small volume elements. This gives our interpolation formula

$$B(\mathbf{r}) = \sum_b m_b \frac{B_b}{\rho_b} W(\mathbf{r} - \mathbf{r}_b), \qquad (A\,3)$$

where the summation is over points (which can be thought of as particles) with the mass assigned to the small volume elements. The crucial point to note is that, if W is a differentiable function, we can calculate the derivatives of B exactly by differentiating (A 3).

The acceleration of any particle requires that we can calculate the pressure gradient.

In a symmetrized form the acceleration for the SPH particle a is

$$\frac{\mathrm{d}\boldsymbol{v}_a}{\mathrm{d}t} = -\sum_b m_b \left(\frac{P_a}{\rho_a^2} + \frac{P_b}{\rho_b^2}\right) \nabla_a W(\boldsymbol{r}_a - \boldsymbol{r}_b), \qquad (A\,4)$$

where the gradients are taken with respect to the coordinates of particle a appearing in W. The reader will find that (A 4) is a particle representation of

$$-\nabla\left(\frac{P}{\rho}\right) - \frac{P}{\rho}\nabla\rho$$

which is $-(\nabla P)/\rho$.

In this way the equations of fluid dynamics are converted into equations for particles. The accuracy of these equations for specific kernels, resolution length h and number of particles can best be estimated by comparison with a wide range of test cases. The integral interpolant (A 2) has dominant errors $O(h^2)$ for kernels similar to the Gaussian and h sufficiently small. The summation interpolant (A 3) has errors which depend on the positions of the particles. Estimates of these errors are that they are $O(h^d \log h)$ in d dimensions. Consistency of the equations requires that h tends to zero more slowly than the particle spacing.

The reader is referred to the cited references for more information.

REFERENCES

ACHESON, D. J. 1990 *Elementary Fluid Dynamics*. Oxford University Press.
BENZ, W. & ASPHAUG, E. 1994 *Icarus* **107**, 98.
BONNECAZE, R. T., HUPPERT, H. & LISTER, J. R. 1993 *J. Fluid Mech.* **250**, 339.
BRITTER, R. E. & LINDEN, P. 1980 *J. Fluid Mech.* **99**, 531.
CAS, R. A. F. & WRIGHT, J. V. 1987 *Volcanic succession*. Chapman and Hall.
CAS, R. A. F. & WRIGHT, J. V. 1991 *Bull. Volcanology* **53**, 357.
CHENG, SIN-I. & SHUBIN, G. 1978 *J. Comput. Phys.* **28**, 315.
CHEONG, H.-B. & HAN, Y.-H. 1997 *J. Oceanogr.* **53**, 179.
CHORIN, A. J. 1967 *J. Comput. Phys.* **2**, 12.
CHOW, E. & MONAGHAN, J. J. 1997 *J. Comput. Phys.* **134**, 296.
DALY, B. J. & PRACHT, W. E. 1968 *Phys. Fluids* **11**, 15.
DIAS, F. & CHRISTODOULIDES, P. 1991 *Phys. Fluids* A **3**, 1711.
DROEGEMEIER, K. K. & WILHELMSON, R. B. 1987 *J. Atmos. Sci.* **44**, 1180.
ELLISON, T. H. & TURNER, J. S. 1959 *J. Fluid Mech.* **6**, 423.
GINGOLD, R. A. & MONAGHAN, J. J. 1997 *Mon. Not. R. Astr. Soc.* **11**, 15.
HAASE, S. & SMITH, R. K. 1989 *Geophys. Astrophys. Fluid Dyn.* **46**, 1.
HALLWORTH, M. A., HUPPERT, H. E., PHILLIPS, J. C. & SPARKS, R. S. J. 1996 *J. Fluid Mech.* **308**, 289.
HUPPERT, H. & SIMPSON, J. E. 1980 *J. Fluid Mech.* **99**, 785.
LIBERSKY, L., PETSCHEK, A. G., CARNEY, T. C., HIPP, J. R. & ALLAHDADI, F. A. 1993 *J. Comput. Phys.* **109**, 67.
LIU, C. & MONCRIEFF, M. W. 1996 *Mon. Weath. Rev.* **124**, 2282.
LONG, R. R. 1956 *Tellus* **8**, 460.
MADER, C. L. 1986 *Numerical Modeling of Water Waves*. University of California Press.
MONAGHAN, J. J. 1992 *Ann. Rev. Astron. Astrophys.* **30**, 543.
MONAGHAN, J. J. 1994 *J. Comput. Phys.* **110**, 543.
MONAGHAN, J. J. 1996 *Physica* D **98**, 523.
MONAGHAN, J. J. 1997a *J. Comput. Phys.* **136**, 298.
MONAGHAN, J. J. 1997b *J. Comput. Phys.* **138**, 801.
MONAGHAN, J. J., BICKNELL, P. & HUMBLE, R. J. 1994 *Physica* D **77**, 217.

MONAGHAN, J. J., THOMPSON, M. C. & HOURIGAN, K. 1994 *The Simulation of Free Surface Flows with SPH*. Adv. Comp. Methods in Fluid Mech. ASME.

MORRIS, J. & FOX, P. 1997 *J. Comput. Phys.* **136**, 214.

ROACHE, P. J. 1997 *Ann. Rev. Fluid. Mech.* **29**, 123.

ROTTMAN, W. & SIMPSON, J. E. 1983 *J. Fluid Mech.* **135**, 95.

SIMPSON, J. E. 1987 *Gravity Currents.* Ellis Norwood.

SIMPSON, J. E. & BRITTER, R. E. 1979 *J. Fluid Mech.* **94**, 477–495.

SMAGORINSKY, J. 1963 *Mon. Weath. Rev.* **91**, 99–164.